IEEE Access
Multidisciplinary | Rapid Review | Open Access Journal

Received May 27, 2021, accepted June 11, 2021, date of publication July 8, 2021, date of current version July 16, 2021.

Digital Object Identifier 10.1109/ACCESS.2021.3095538

Extendable Array Rectenna for a Microwave Wireless Power Transfer System

JEONG-MIN WOO[1], WONSEOB LIM[1], JONGSEOK BAE[2], CHAN MI SONG[2], KYOUNG-JOO LEE[1], SANG-HWA YI[1], (Member, IEEE), AND YOUNGOO YANG[2], (Senior Member, IEEE)

[1]Korea Electrotechnology Research Institute, Seongsan-gu, Changwon-si, Gyeongsangnam-do 51543, South Korea
[2]Department of Electrical and Computer Engineering, Sungkyunkwan University, Suwon 16419, South Korea

Corresponding author: Wonseob Lim (skysyub116@keri.re.kr)

This work was supported by the Korea Electrotechnology Research Institute (KERI) Primary Research Program through the National Research Council of Science and Technology (NST) funded by the Ministry of Science and ICT (MSIT) under Grant 21A01040.

ABSTRACT In this study, a rectenna is adopted in a microwave-based wireless power transfer system to rectify the received radio frequency (RF) to DC power. Each rectenna comprises a DC-DC converter at the DC output port to ensure a stable power supply and a Schottky diode for the DC-combining network. The results indicate that the RF-DC conversion efficiencies of the rectifier circuit and 4 × 1 rectenna were 71% and 71.2% when the unit-cell RF input levels were 19 dBm and 19.6 dBm, respectively. Furthermore, the DC output levels of a 4 × 8 rectenna with and without the DC-DC converter were 28 V and 30 V, respectively, when the unit-cell RF input level was 20.2 dBm. Additionally, the RF-DC conversion efficiencies were 52.6% and 59.9% with and without the DC-DC converter, respectively. Thus, we experimentally verified that the Schottky diode combined with the DC-DC converter at the DC output port can increase the DC power combining level, making it suitable as an extendable array rectenna system.

INDEX TERMS Rectenna, Schottky diodes, wireless power transmission.

I. INTRODUCTION

The increasing demand for various applications, such as smart home systems, health monitoring, electric vehicle charging, implantable electronic devices, and sensors has resulted in the rapid development of wireless power transfer (WPT) technology [1]–[8]. Transmission of wireless energy results in highly compact and user-intuitive systems. WPT technology can be divided into two categories, namely non-radiative and radiative. A popular non-radiative source is a magnetic field generated by a conductive coil system, wherein power is transferred to another coil via inductive coupling. This system is implanted in smartphones and various Internet-of-Things systems owing to its high transfer efficiency of approximately 70% within a proximity of a few centimeters [9]; beyond this, the power transfer efficiency decreases due to poor coupling. The efficiency can be improved by increasing the coil diameter; however, a physical size limitation exists. Therefore, WPT technology based on radiation is adopted for distances longer than a few meters. Radiative WPT systems comprise two components, namely a transmitter and a receiver. In the transmitter, a magnetron or solid-state power amplifier is used for the generation of the electromagnetic field, and the antenna facilitates free-space radiation. The radiated microwave from the transmitter diverges as it transmits through free space. However, the transfer loss in free space increases with the increase in the transmission distance. Several researchers extended the distances to thousands of kilometers to investigate solar-powered satellites [10]. Typically, a phased array is adopted in both transmitter and receiver antennas to reduce the transfer loss. To receive a certain power level without increasing the transmitting power, a large-scale phased array antenna system is preferred. This can enhance the antenna gain, thereby reducing the transfer loss.

The receiver comprises an antenna and a radio frequency (RF)-DC rectifying system, which converts RF energy into electrical energy. Previously, multiple antenna shapes and different circuit topologies were adopted to increase the receiver performance. A power amplifier, voltage doubler, power combiner, and impedance matching techniques were developed to account for the different input

The associate editor coordinating the review of this manuscript and approving it for publication was Tariq Masood.

power levels, thereby increasing the RF-DC conversion efficiency [11]–[16]. Multiple-band and three-dimensional (3D) wide-angle structures were studied to improve the antenna usability and gain in various scenarios [17]–[21]. To reduce the connection loss in the receiver system, a rectenna was developed, comprising a receiving antenna and a rectifying circuit on the front-side and back-side of a single printed circuit board (PCB), respectively. Previous studies on rectenna were primarily based on packaged diode type rectennas that generate parasitic components and rectification losses. Recently, the use of bare Schottky diodes for higher efficiency and high-power has been reported [22], [23]. Furthermore, RF-DC conversion efficiency of 73.1% was achieved with the rectifying circuit by using a common-ground and multiple-stack structure based on a bare Schottky diode [24].

To receive higher amounts of power from the transmitter, the number and size of the rectenna need to be increased. However, the loss of the matching network in the rectenna array increases owing to the multiple circuit components. Therefore, reconfigurable DC output connections (series, parallel, and series–parallel) and RF combining techniques were studied to determine the best strategy using RF signal connections and output power lines. A comparison of the DC output and RF-combined output verified that the RF combination exhibits a higher efficiency in a low input power range with additional loss in longer feeding lines [25]. Furthermore, the comparison of single and array rectenna performances indicated that the array rectenna exhibits a higher voltage with reduced conversion efficiency [26]. Although the series–parallel connection is a popular choice for designing a DC output [27], the conversion efficiency of parallel DC connection is 1% higher than those of the series and series–parallel connections [28]. However, the non-linearity of each rectenna increased with the scaling law, regardless of the DC or RF combining methods [29]. Thus, increasing the RF-DC conversion efficiency is challenging owing to the multiple-input and multiple-output implementation in WPT systems.

In this study, we investigated the extendable rectenna based on the Schottky diode connected to the DC-DC converter at the DC output port. Existing studies have reported that the output voltage fluctuates based on the input power level, which can limit the usability of the rectenna. To overcome this limitation, we developed a single DC-DC converter combined with a rectenna. The array rectenna is a parallel combination of using DC-DC converter rectennas. The Schottky diode connected in series to a DC-DC converter at the DC output port. This stabilized the output voltage level regardless of the input power level in the array connections, which can be utilized as an extendable array rectenna based on the input RF beamforming width.

II. DESIGN AND FABRICATION

Both transmitter and receiver antennas were designed based on the right-hand circular polarization (RHCP) at 5.8 GHz. Typically, a microwave receiver comprises an antenna, a matching network, Schottky diode-based RF-DC rectifier, DC power line, DC-DC converter, and Schottky diode.

A. ANTENNA DESIGN

Based on a previous study by Oraizi [30], we developed an RHCP patch antenna to operate at 5.8 GHz considering fractal geometry. Fig. 1 depicts the schematic view and Table 1 lists the design parameters of the patch antenna. The unit-cell size was half the wavelength of the incident wave to design an antenna of compact size. We used a 1.52-mm-thick dielectric substrate, Taconic RF-35, with a dielectric constant of 3.5 and a loss tangent of 0.0018 at 5.8 GHz. The feed point illustrated in Fig. 1(a) is obtained by a through-via hole. It indicates the location where the return loss was suppressed and optimized, and the axial ratio was nearly 0 dB. The RHCP gain of this single patch was 6.429 dBic at 5.8 GHz.

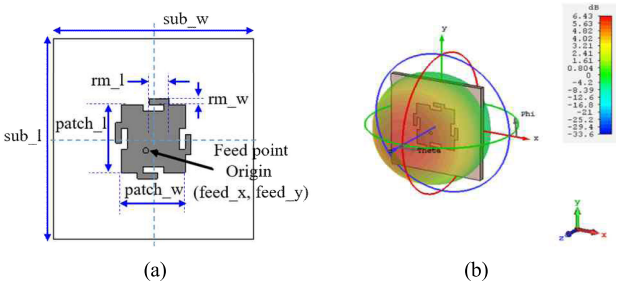

FIGURE 1. (a) Schematic of the right-hand circular polarization (RHCP) patch antenna. (b) Simulated result of the 3D radiation pattern at 5.8 GHz.

TABLE 1. Design parameters of the RHCP patch antenna.

Parameter	Value (mm)
patch_w	10.86
patch_l	11.5
rm_l	3.33
rm_w	1
feed_x	−1.3
feed_y	−2
sub_w	25.845
sub_l	25.845

To verify the generation of the RHCP, the surface current distributions on the fractal patch were simulated at a time period (T) of 5.8 GHz (Fig. 2). The simulation was performed using a 3D electromagnetic (EM) simulator, namely the CST Microwave Studio Suite software. Fig. 2 depicts the simulated surface current distributions observed from the +z-direction at $t = 0$, $T/4$, $2T/4$, and T. At $t = 0$, the major currents increase on the left and right grooves of the patch, and their vector sum points from the upper side to the lower side. At $t = T/4$, the major currents exist on the upper and lower grooves of the patch, generating a vector sum that points from the left to the right of the patch. This vector sum is orthogonal to that at $t = 0$ and rotates counterclockwise as the value of t increases, thereby generating the RHCP.

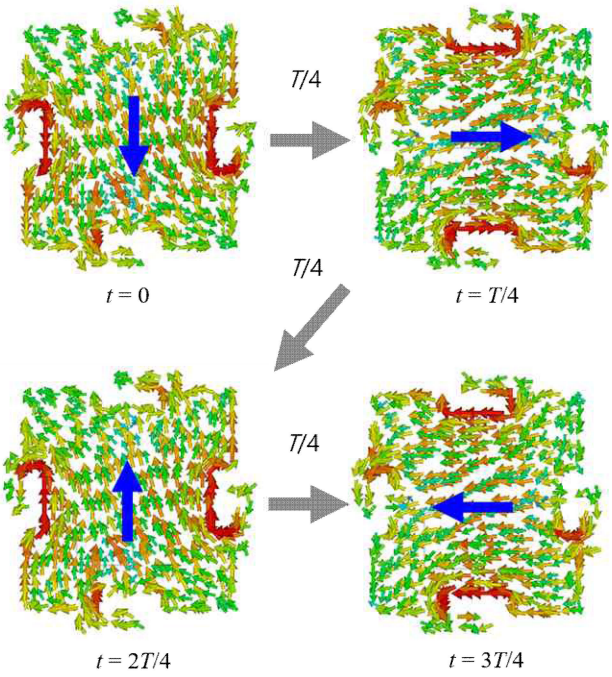

FIGURE 2. Simulated surface current density of the fractal patch antenna.

Fig. 3(a) illustrates an 8 × 8 array antenna composed of the fractal patch depicted in Fig. 1. Fig. 3(b) depicts the receiving power at 5.8 GHz based on the spacing (d) between patches when the receiver antenna is composed of the patch array antenna. Herein, the transmitter antenna was set with an RHCP gain of 22.8 dBic and a 3 dB beamwidth of 12.6 °. Additionally, the transmitter and receiver are located 1 m apart in front of each other, considering the scale model. The power transmitted from the transmitter was set to 100 W. Based on the simulation, the maximum receiving power was attained between 0.65 and 0.75 λ. This is because the size of the entire receiver array increases as the spacing increases. Therefore, the gain and receiving power of the receiver antenna increase. However, when the spacing exceeds 0.8 λ, the number of array elements within the width of the transmission beam decreases, which in turn decreases the receiving power rapidly. Considering the maximization of the received power and the possibility of fabricating the array antenna, a 4 × 8 patch array with 0.658 λ spacing was designed as a unit array for the receiver, as depicted in Fig. 4.

To validate the performance of the designed 4 × 8 array antenna of each patch element, we fabricated a 4 × 8 patch array antenna with 30 dB isolation between the cells, as depicted in Fig. 5. A rigid coaxial cable was attached to obtain the measurements in the anechoic chamber. Fig. 6 illustrates the simulation and measurement results of element no. 12 (Fig. 5). The simulated and measured reflection coefficients were approximately −10 dB at 5.8 GHz as depicted in Fig. 6(a). Fig. 6(b) illustrates the RHCP-realized gain and axial ratio (AR) in the +z-direction and the RHCP gain and AR measured at 5.8 GHz, which were 6.98 dBic

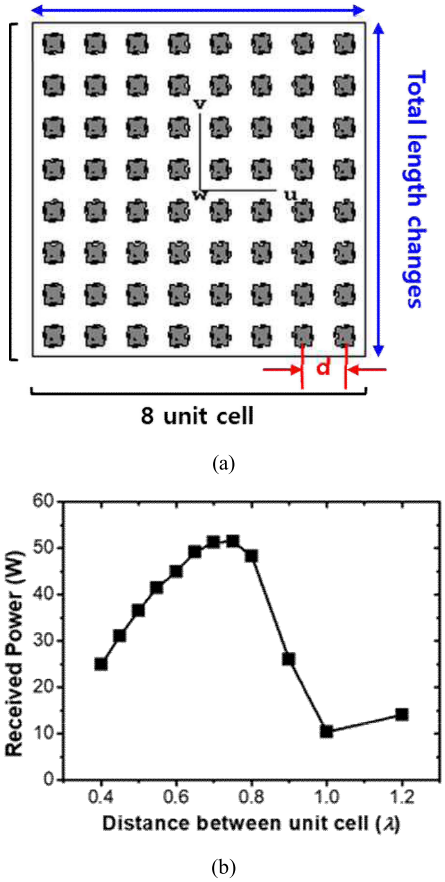

FIGURE 3. (a) Schematic view of the receiving 8 × 8 fractal patch array antenna. (b) Received power depends on the spacing (d) between the patch elements.

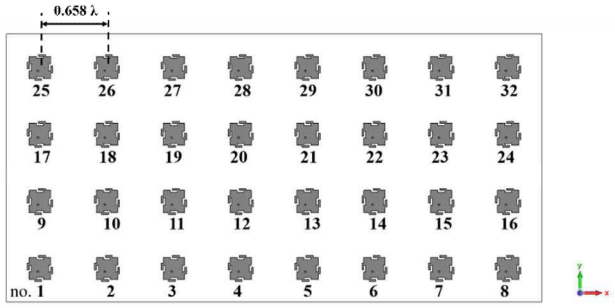

FIGURE 4. Schematic view of the 4 × 8 patch array with 0.658 λ spacing.

and 2.99 dB, respectively; these results concur with those of the simulation. Additionally, both normalized radiation patterns in the x–z and y–z planes exhibit a similar tendency, as depicted in Figs. 6(c) and 6(d), respectively. Therefore, the proposed 4 × 8 patch array unit can receive RF power with high efficiency for wireless RHCP at 5.8 GHz.

B. RECTIFYING CIRCUIT DESIGN

The rectifying circuit can be designed using various topologies, such as a series-connected diode, parallel-connected diode, full-bridge circuit based on four diodes, and voltage

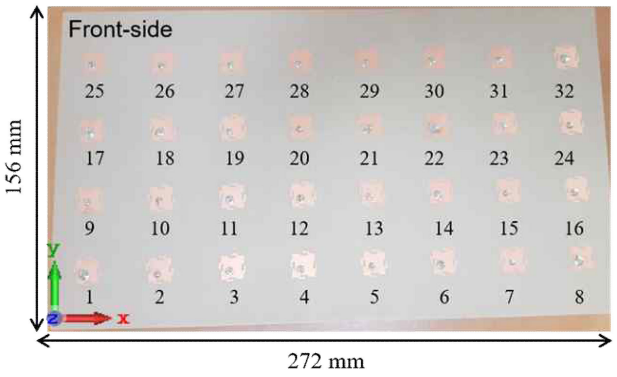

(a)

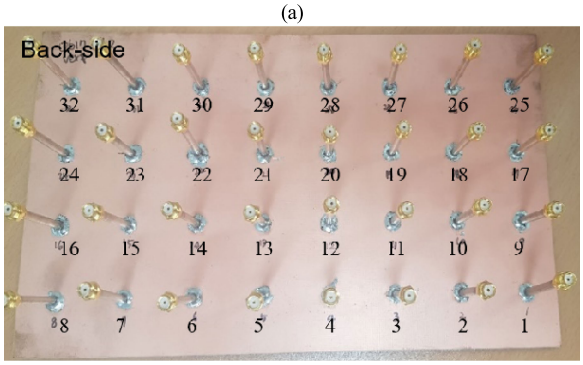

(b)

FIGURE 5. **Photographs of the (a) front-side and, (b) back-side of the fabricated antenna.**

doubler based on two diodes [13]. Among these, the voltage doubler can be expanded to configure a multi-stage doubler that generates a higher output voltage. Fig. 7 illustrates the Greinacher voltage doubler adopted in this study to obtain the rectifying circuit. As the voltage applied to the circuit is a sine wave, a negative half-wave is applied to diode D_1, which charges the capacitor C_{IN} to voltage V_1. The subsequent positive half-wave is applied to diode D_2. Finally, the C_{LOAD} is charged twice that of V_1. The single-stage doubler was stacked in parallel to implement a four-stage doubler.

The rectifying circuit comprises an impedance matching circuit based on the PCB transmission line to maximize the RF-DC rectifying efficiency. The rectifying efficiency was calculated using the equation $\eta = P_{DC}/P_{RF}$, where P_{DC} denotes the output DC power delivered to the load impedance, and P_{RF} indicates the input RF power. The circuits were designed using the ADS software and then optimized. Both the shunt capacitor and low-frequency band-pass filter were selected to reduce the noise signal and reflection coefficient, respectively, and match 50 Ω. Existing studies use packaged Schottky diodes in the rectifiers. Conversely, the proposed rectifier circuit comprises a voltage doubler topology based on the bare-die type Schottky diode. It has a low turn-on voltage of approximately 0.4 V, which reduces the power consumption and increases the RF-DC rectifying

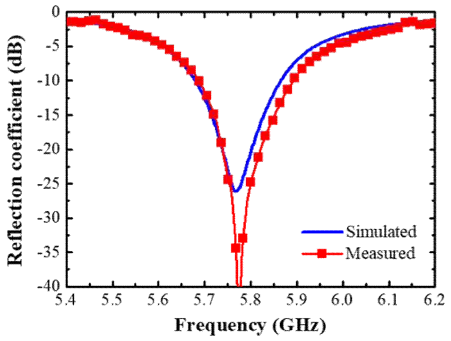

(a)

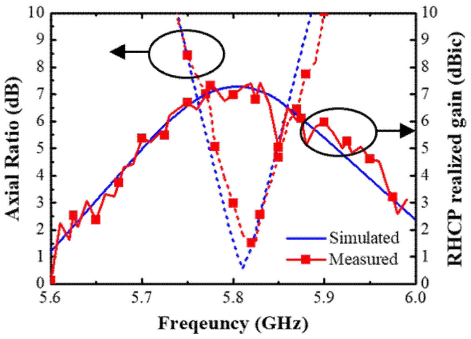

(b)

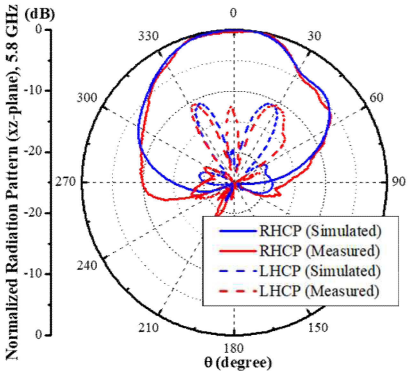

(c)

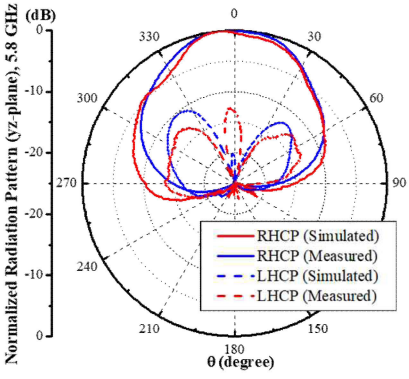

(d)

FIGURE 6. **Comparison between simulated and measured results of element no. 12 in the patch array. (a) Scattering parameter and the (b) axial ratio and right-hand circular polarization (RHCP)-realized gain. Radiation pattern in the (c) x–z plane and (d) y–z plane.**

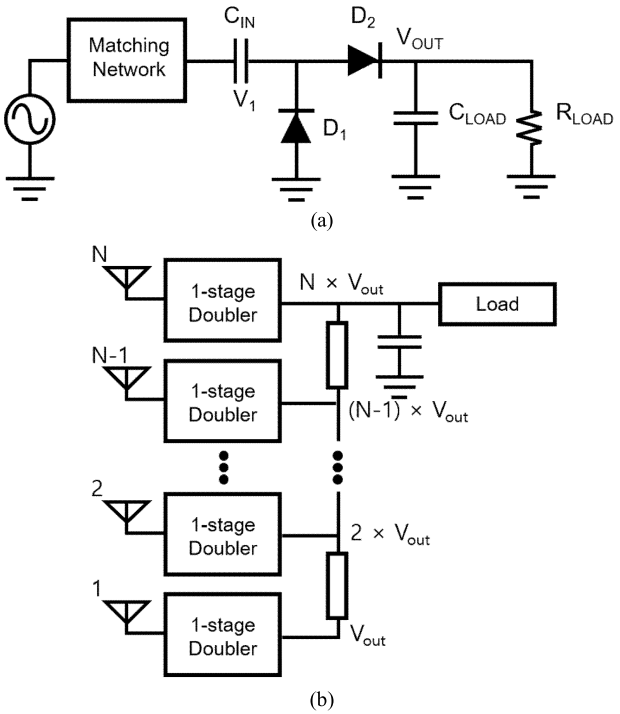

FIGURE 7. Schematic of (a) a 1-stage doubler and (b) an N-stage doubler.

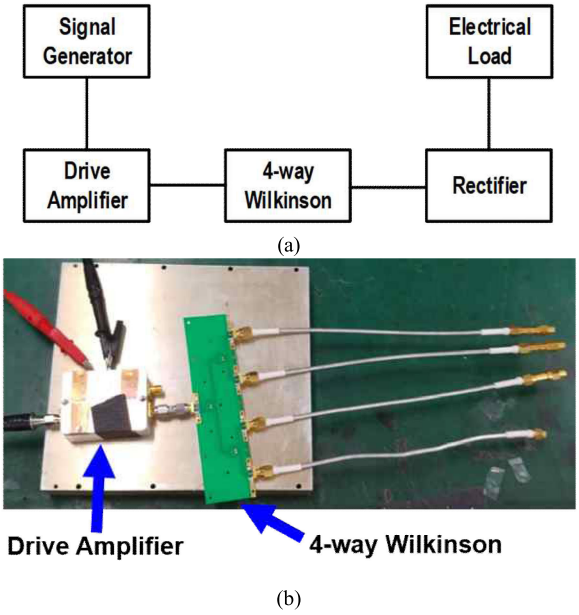

FIGURE 8. Measurement setup: (a) Schematic view and (b) photograph.

efficiency. As the reported rectifying efficiencies were saturated, a bare-die type Schottky diode was adopted to reduce the parasitic component values and increase the efficiency. Fig. 8 depicts the measurement setup comprising a drive amplifier and a four-way Wilkinson divider to supply the RF power to the rectifier; the electric load was used to measure the DC output power.

Macom MA4E-1319 is an unpackaged gallium arsenide substrate-based Schottky diode. Figs. 9 and 10 depict the photographs of the wire-bond diode and measured results of the MA4E-1319-based rectifying multi-stage doubler, respectively, as presented in a previous study [24]. The substrate material is RF35 with a thickness of 520 μm. As illustrated in Fig. 10, the peak efficiency was 71% at 19 dBm, and the highest efficiency was 73% at 22 dBm. The output DC voltage was approximately 30 V at 19 dBm with a four-stage doubler. Additionally, the bare-die type was compatible with the surface-mount technology owing to the wire bonding depicted in Fig. 9.

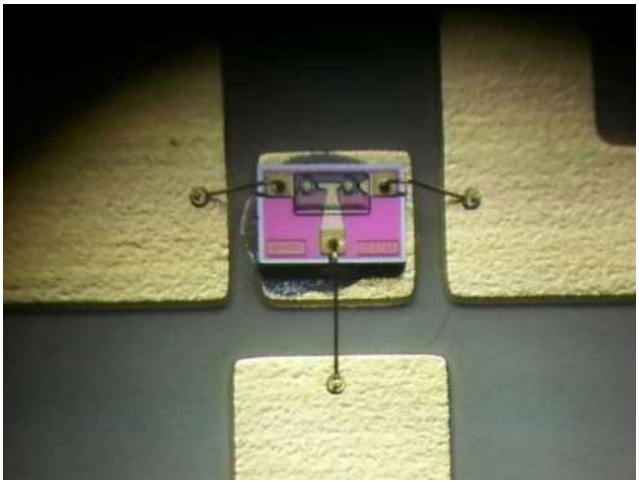

FIGURE 9. Photographs of the wire-bond diode at the rectifier circuit.

C. RECTENNA IMPLEMENTATION

As mentioned in Section I, a rectenna comprises a receiving antenna and rectifying circuit on the front-side and back-side of a single PCB, respectively. Fig. 11 illustrates the rectenna thickness of the multi-layer PCB structure. The layers include an antenna, RF ground plane, DC ground plane, and rectifier. The RF and DC ground planes are connected by the through-via hole, VIA1, at the edge of the PCB. VIA1 disconnected from the M2 and M3 layers at the center of the PCB. It is perforated from the M1 to M4 layers to provide RF signal feeding. VIA2 provides a common ground to the rectifier circuit and DC-DC converter on the M4 layer. The final ground line is connected to the ground.

As depicted in Fig. 12, the proposed rectenna of dimensions 156 mm (H) × 272 mm (L) comprises 32 unit-cells in a 4 × 8 array. Each unit-cell antenna at the front is connected to the Schottky diode at the backside by a through-via hole. Further, four units of diodes were stacked in a group at the backside to obtain a four-stage voltage doubler. Eight parts of the DC output power from the rectifier were connected to a DC-DC converter to prevent the output voltage fluctuation, which relies on the input power level. The model LT3434 DC-DC converter was utilized with a wide input range of up to 60 V and a peak switch current of 3 A. The

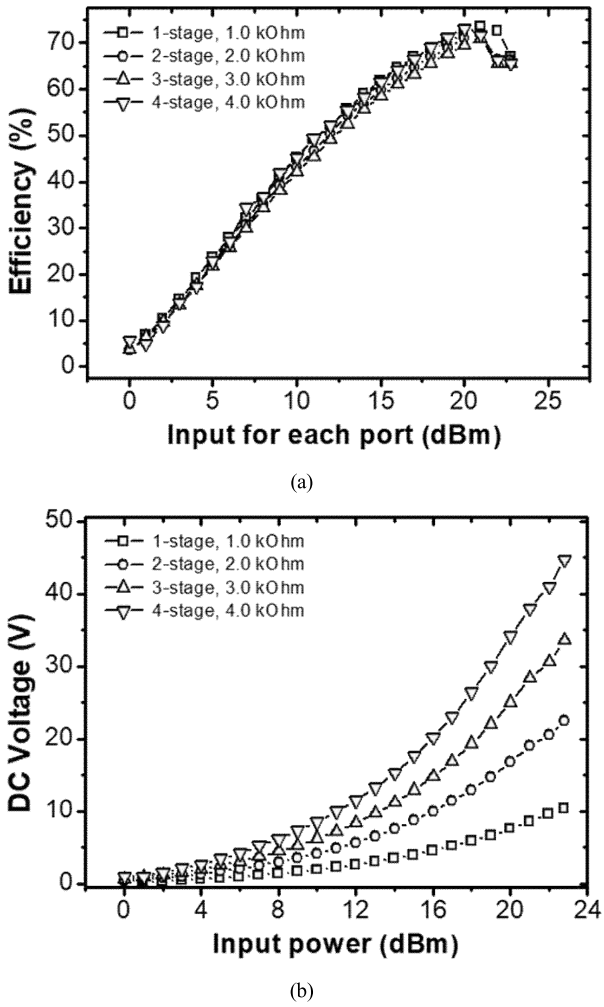

FIGURE 10. Measurements obtained from a multi-stage doubler based on MA4E-1319 diode: (a) Efficiency and (b) DC output voltage.

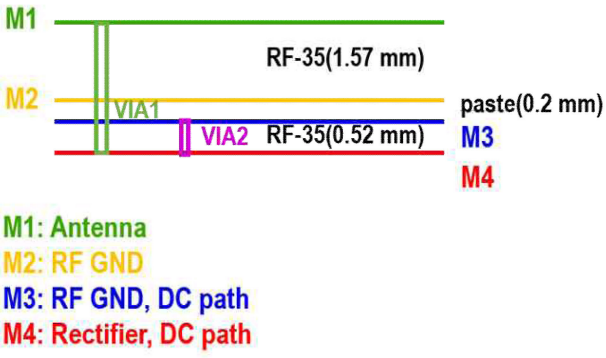

FIGURE 11. Schematic of the multi-layer printed circuit board (PCB) information.

efficiency is expected to be more than 85% when the input voltage is higher than 30 V with a 28 V output voltage. The output voltage was configured using the feed-back resistor of the DC-DC converter.

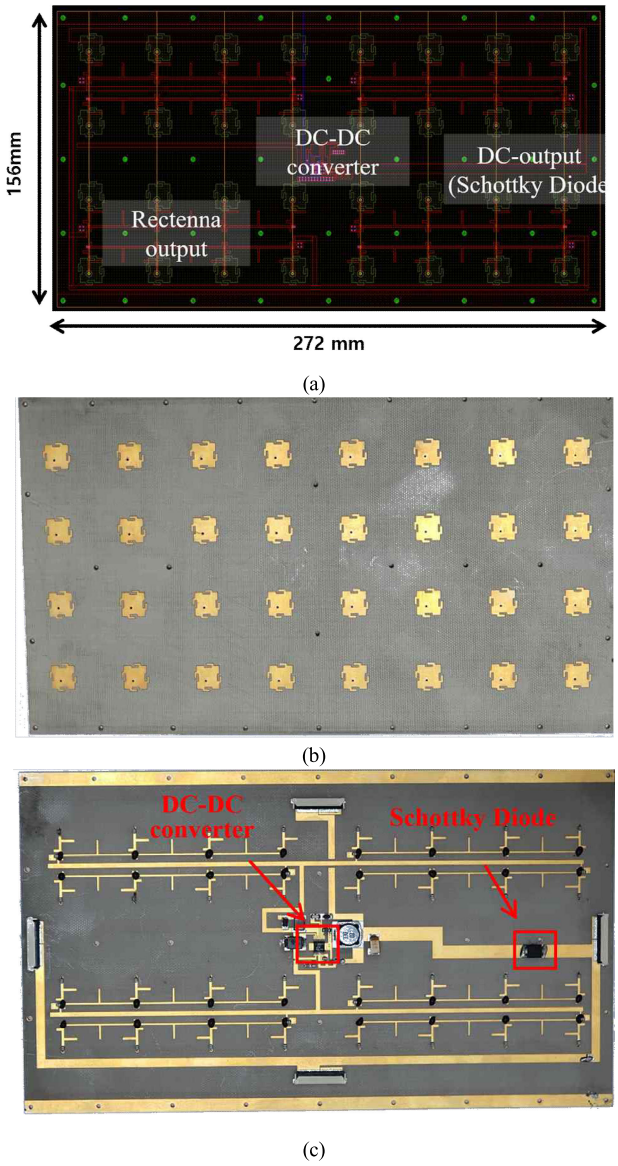

FIGURE 12. (a) Schematic of the rectenna structure. Photographs of the (b) front-side and (c) the backside.

A simulation was performed to verify the antenna performance of the proposed rectenna. Fig. 13 illustrates the simulated results of the scattering parameter, axial ratio, and realized RHCP gain of the central patch element in the rectenna array. The rectenna model in the simulation includes the antenna structure with the rectifying circuit. In comparison with the antenna-only structure, the reflection coefficient of the patch of the proposed rectenna satisfies the condition of less than −10 dB at 5.8 GHz. Additionally, its axial ratio nearly equals 0 dB owing to the through-via hole, which is similar to that of the antenna-only case.

III. RESULTS AND DISCUSSION

A. SINGLE RECTENNA

The performance of the rectenna was evaluated with MA4E-1319 in an anechoic chamber. The transmitter comprises

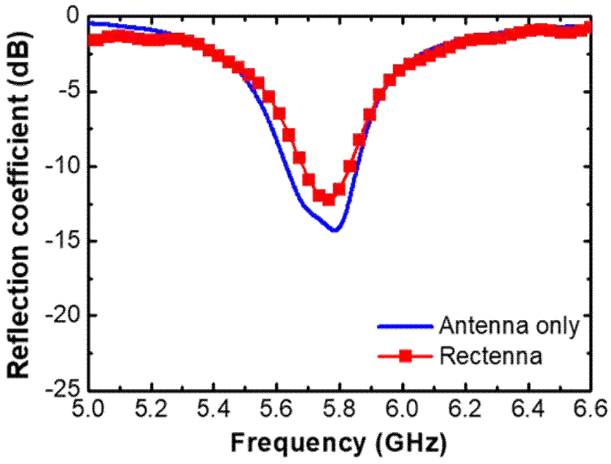

(a)

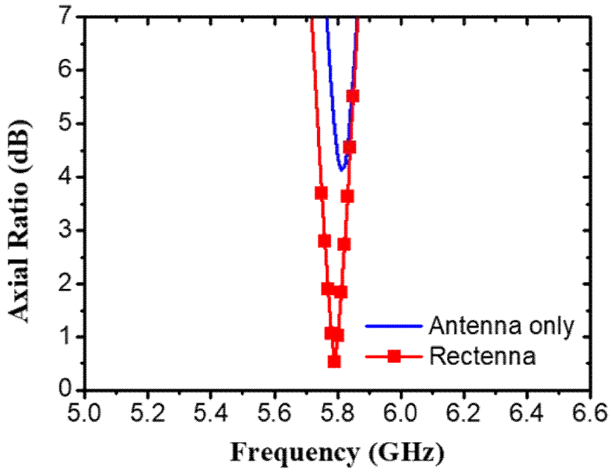

(b)

FIGURE 13. Simulated electromagnetic response of the rectenna: (a) Reflection coefficient and the (b) axial ratio.

power-amplifier modules, wherein each channel amplifies the RF signal from a signal generator and controls the 6-bit phase shifters. The total output power was 1.2 kW, and the dimensions of the transmitter antenna were 1.8 m × 1.2 m with an RHCP gain of 16.5 dBic. The received RF power was controlled by the transmitter power and the distance between the transmitter and receiver. Fig. 14(a) depicts the customized automatic jig system of dimensions 2.5 m × 2.2 m with 8 columns and 16 rows. A maximum of 128 rectennas were available to configure the jig system. We used acetal plastic, which has a low dielectric constant of approximately 3.7 and strong mechanical strength, for the configuration. Additionally, a remote motor controller with 0.5 ° motor step was used to determine the best alignment between the transmitter and receiver for generating the maximum RF transfer efficiency. Fig. 14(b) depicts the rectenna installed on the left-side with and without the DC-DC converter. The RHCP antenna without a rectifying circuit was installed on the right-side to confirm the input RF power to the receiver.

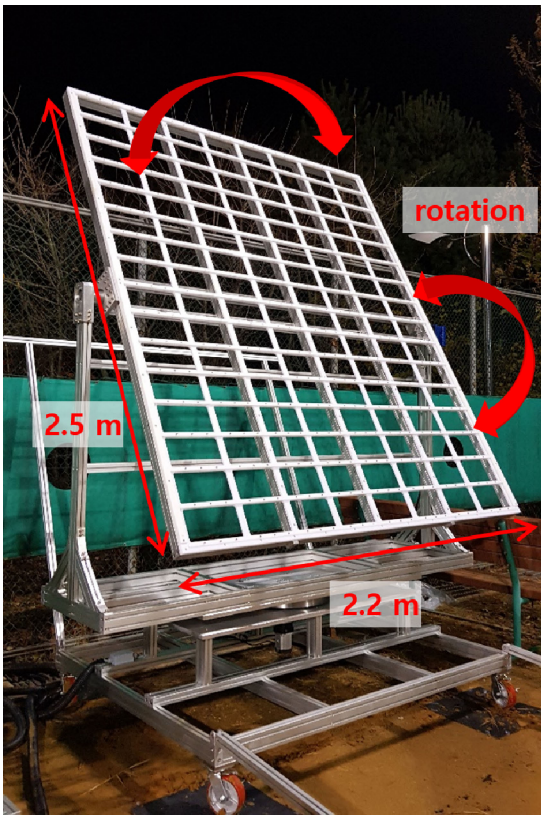

(a)

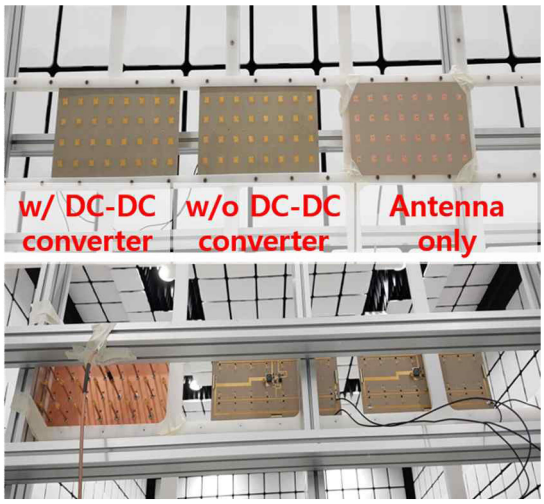

(b)

FIGURE 14. (a) Automatic rectenna jig system. (b) Single rectenna installation.

The incident RF power was measured for each unit-cell using an RHCP antenna without a rectifying circuit. The power distribution, which varied based on the changing magnitude of the incident power, was measured each time. Fig. 15 depicts the 4 × 8 rectenna divided into eight 4 × 1 rectennas. A total of four 4 × 8 rectennas were used to measure the DC output power of the 4 × 1 rectenna in each zone, and the DC output power was measured by

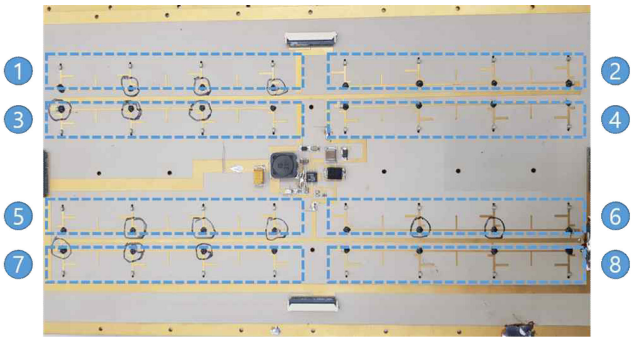

FIGURE 15. 4 × 8 rectenna divided into eight 4 × 1 rectennas.

TABLE 2. DC output power of 4 × 1 rectennas.

Number of section (4 × 1 rectenna)	Input Power (W)	4 × 8 rectenna #1	4 × 8 rectenna #2	4 × 8 rectenna #3	4 × 8 rectenna #4
①	0.382	0.23	0.20	0.25	0.24
②	0.383	0.22	0.19	0.25	0.23
③	0.444	0.24	0.24	0.18	0.26
④	0.445	0.18	0.18	0.22	0.24
⑤	0.455	0.15	0.22	0.26	0.27
⑥	0.416	0.24	0.28	0.27	0.26
⑦	0.365	0.20	0.26	0.19	0.23
⑧	0.356	0.18	0.20	0.20	0.22

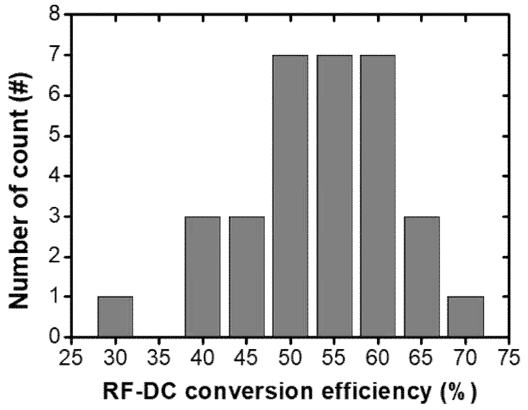

FIGURE 16. Distribution of 4 × 1 rectenna RF-DC conversion efficiency.

the electric load. Table 2 lists the performance of thirty-two 4 × 1 rectennas, and the maximum RF-DC conversion efficiency was 71.2% at 19.6 dBm. As the rectifier circuit efficiency was 71% at 19 dBm, the rectenna exhibited a similar result. Fig. 16 illustrates the distribution of the rectenna performance around an RF-DC conversion efficiency of 55%, which can be attributed to the impedance mismatching owing to each slightly different diode specification.

Fig. 17 illustrates the measurement results of the single 4 × 8 rectenna with and without the DC-DC converter. As indicated in the figure, the output power exhibits a gentle

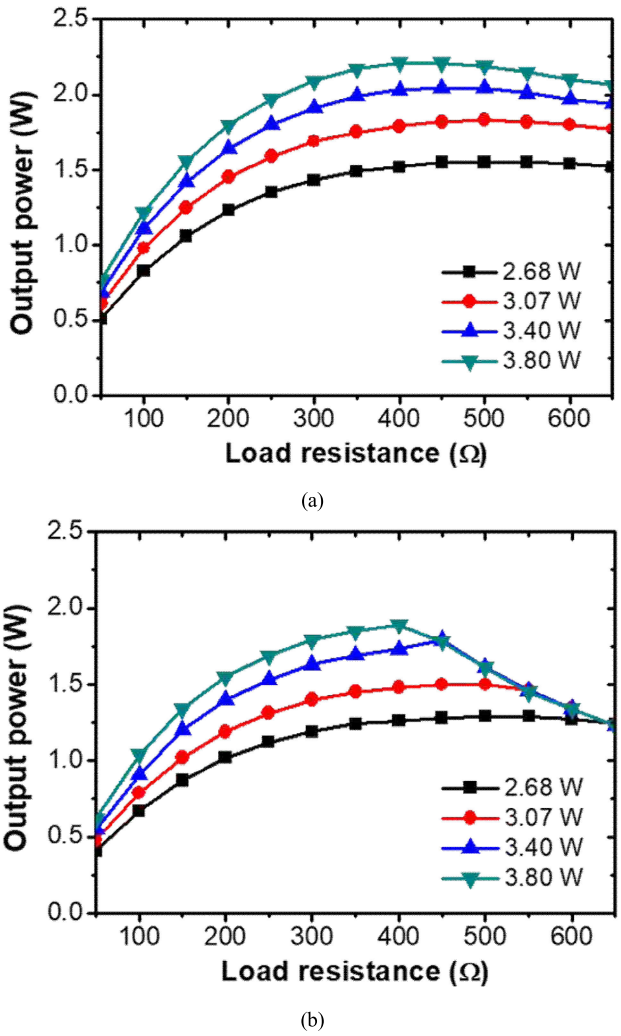

FIGURE 17. Rectenna DC output power measurement, (a) without DC-DC converter and (b) with DC-DC converter.

downward curve above 450 Ω without the DC-DC converter. The highest RF-DC conversion efficiency was 59.9% at 20.2 dBm, and the DC output power measured was 2.04 W with 30 V. Conversely, the measured DC output power was 1.79 W with 28 V at a load impedance of 450 Ω and 20.2 dBm input RF power with the DC-DC converter. The calculated RF-DC conversion efficiency was 52.6%, and the DC-DC converter efficiency was approximately 80-88% based on the input power. The rectenna with the DC-DC converter exhibits decreased efficiency. However, when the rectenna with the DC-DC converter generates an output voltage of approximately 28 V, it remained stable regardless of the input power.

B. SCHOTTKY DIODE AT THE RECTENNA OUTPUT PORT

As the 3 dB beamwidth and the radiation pattern of the transmitted beam can change owing to the excited phase of the transmitter, the receiving configuration and the DC output connection must be extendable as desired. Furthermore,

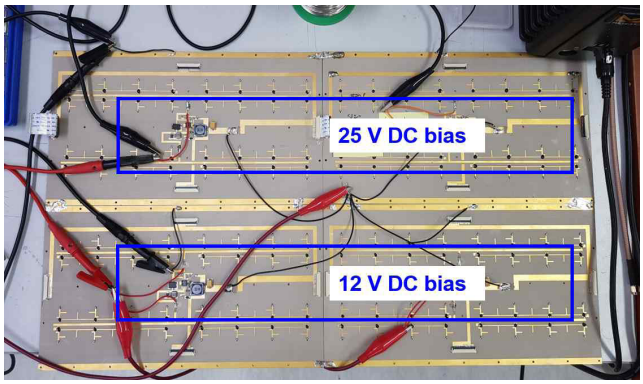

FIGURE 18. Experimental setup of the rectenna with variations in power supply.

the output voltage of the rectenna array should be stable regardless of the array rectenna configuration. Fig. 18 depicts a varying input power applied to the array rectenna connected in parallel. We utilized a power supply to control the parameter accurately. The experiments were performed under the following four conditions. First, DC power of 25 V was supplied to both upper and lower rows of the rectenna. Second, 25 V and 12 V DC powers were supplied to the upper and lower rows, respectively. Herein, the upper rectenna was operated under normal conditions, whereas the lower rectenna was operated in an unstable condition. As the load impedance decreased at 12 V, the required current increased; however, the current was limited to 500 mA. Third, 8.5 V DC power was supplied to both the upper and lower rows of the rectenna under unstable operating conditions. Herein, the currents of both rows were limited owing to insufficient power. Fourth, 8.5 V DC power was supplied to the upper row, whereas no power was supplied to the lower row.

Consequently, when multiple DC-DC converters were operated under normal conditions, the DC-DC converter with the highest voltage drove all the loads and operated dominantly, and the power was not supplied to other DC-DC converters. Owing to the variations in the output feedback resistance caused by the fabrication error, the output voltage differs for each DC-DC converter despite identical design parameters, which leads to the operation of a single DC-DC converter among the four converters. As summarized in Table 3, the DC-DC converter operates excellently in case 1 with sufficient power. When insufficient power is applied, multiple DC-DC converters begin to operate with lower efficiencies, as in cases 2, 3, and 4. Therefore, when the current is not sufficiently supplied toward the DC-DC converter, the rectenna efficiency decreases as it does not receive an appropriate amount of power.

To overcome this limitation, a Schottky diode was adopted in series at the backstage of the DC-DC converter in the DC output port. We adopted a package SMC type Schottky diode from Vishay Semiconductors, VS-30BQ100-M3, with a turn-on voltage of 0.62 V, breakdown voltage of 100 V, and an average forward current of 3.0 A. Fig. 19 depicts the three

TABLE 3. Comparison of power supply variations.

	Case 1 25 V, 25 V	Case 2 25 V, 12 V	Case 3 8.5 V, 8.5 V	Case 4 8.5 V, off
Load (Ω)	52	20	12	12
Power (W)	8.2	6.7	5.5	2.3
Vout (V)	20.3	11.6	8.1	5.3

TABLE 4. Comparison of different operating conditions in the rectennas.

	Case 1 Normal+Normal			Case 2 Normal+Off (Without Schottky diode)			Case 3 Normal+Off (With Schottky diode)		
	1	2	1 + 2	1	2	1 + 2	1	2	1 + 2
Load (Ω)	3 k	3 k	1.5 k	1 k	-	1 k	1 k	-	1 k
Power (W)	0.26	0.25	0.54	0.8	-	0.68	0.8	-	0.8
Vout (V)	28.6	28.4	29.1	28.7	-	26.4	28.7	-	28.7

experimental cases conducted in this study. First, two rectennas were installed without a Schottky diode and operated normally. Second, the rectenna without the Schottky diode was operated normally, whereas nearly no input power was supplied to the other rectenna. Third, the rectenna was tested with the Schottky diode under conditions identical to those of case 2. Table 4 summarizes the obtained experimental results. In case 1, the output power summation operates normally. In case 2, the absence of the Schottky diode decreases the summation of the power and voltage. In case 3, the presence of the Schottky diode conserves the output power and voltage adequately in the summation. This can be attributed to the Schottky diode conducting the forward current and blocking the reverse current, which in turn operates the DC-DC converter in the normal power summation.

C. ARRAY RECTENNA

We conducted an outdoor experiment using a large array rectenna based on 128 4 × 8 rectennas. As depicted in Fig. 20, each rectenna comprised a DC-DC converter connected in parallel to the load. The Schottky diode at the output port was also adopted in each rectenna to facilitate DC combining. The best alignment or angle between the transmitter and receiver was determined to obtain the maximum RF transfer efficiency. As the distance between the transmitter and receiver increased, the ground reflections became larger. Therefore, the distance was set to 50 m, as depicted in Fig. 21(a). We used the same transmitter system as in the single rectenna.

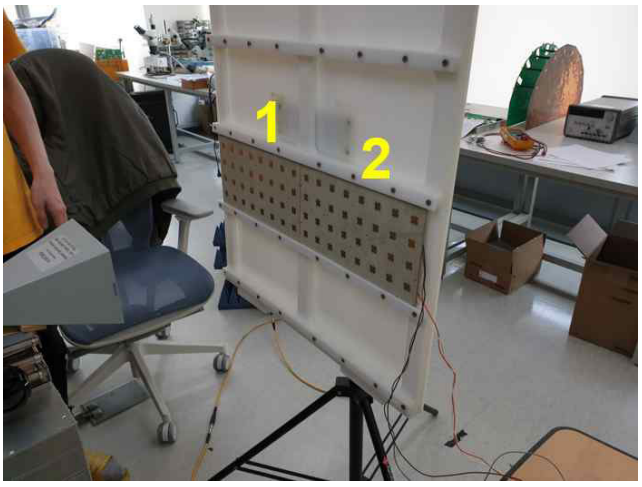

(a)

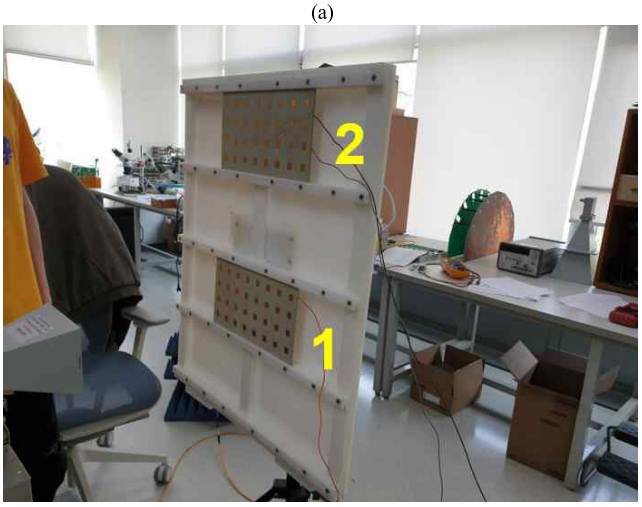

(b)

FIGURE 19. Photographs of the rectenna experiments. (a) The two rectennas are under normal conditions. (b) One rectenna is under normal condition and the other rectenna is turned off.

TABLE 5. DC output power of each line.

	Power (W)		Power (W)
Line 1	0.74	Line 9	2.00
Line 2	2.37	Line 10	1.09
Line 3	2.78	Line 11	0.46
Line 4	2.48	Line 12	0.37
Line 5	2.78	Line 13	0.05
Line 6	2.16	Line 14	0.18
Line 7	2.53	Line 15	0.17
Line 8	2.41	Line 16	0.08

The input RF power for the receiver was set to 16 dBm for the central rectenna.

Table 5 lists the results of each DC output power line. As shown in Fig. 21(b) and (c), a flat-flexible circuit cable was connected to each rectenna in the horizontal direction,

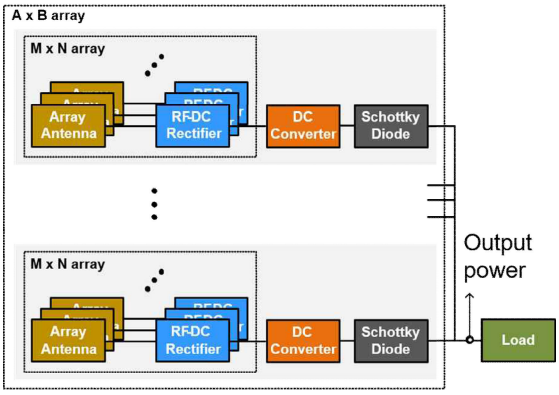

(a)

(b)

FIGURE 20. (a) Schematic of the array rectenna system. (b) Photograph of the array rectenna system.

TABLE 6. Comparison of results obtained in different studies.

Ref. no.	Freq. (GHz)	Number of rectenna unit	Single rectenna conversion efficiency	Connection
[26]	5.8	16 (4 × 4)	71.2%	Series-parallel
[28]	2.45	4 (2 × 2)	-	Series / parallel / Series-parallel
[31]	5.8	30 (3 ×10)	44.1%	Series / parallel
[32]	5.8	25 (5 × 5)	66.2%	Series-parallel
This work	5.8	4 (4 × 1) /32 (4 × 8)	71.2% /59.9%(w/o DC converter) /52.6%(w/ DC converter)	Parallel

and the DC cable was connected at the end. Each DC cable was connected or disconnected in the control box, as depicted in Fig. 21(d). Eight rectennas were connected in parallel,

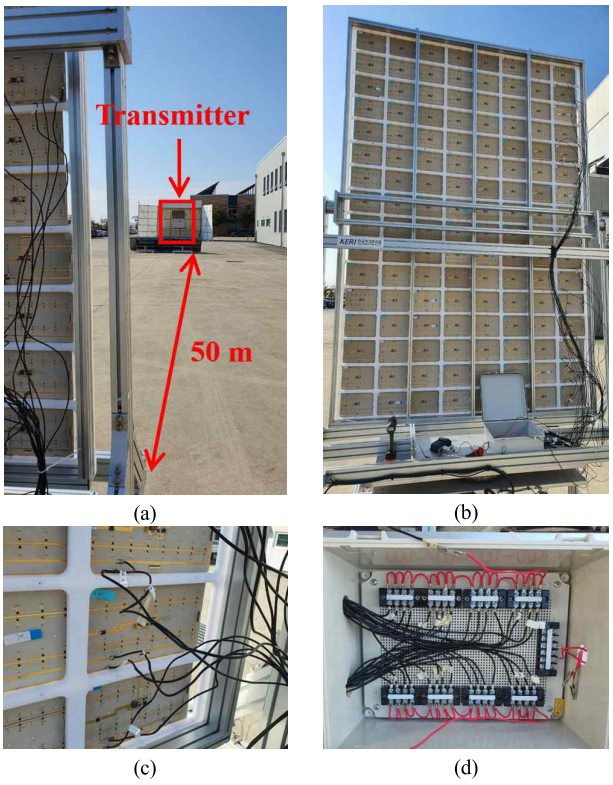

FIGURE 21. Photographs of (a) the transmitter and receiver during the outdoor experiment; (b) back-side of the array rectenna system; (c) DC-summation in the horizontal connection; and (d) the 16-line DC-summation in the control box.

FIGURE 22. Measurement of the total summation.

comprising one line. Sixteen such lines were compared and added, generating an 8 × 16 array or 128-rectenna summation. All lines were connected in parallel and measured, as depicted in Fig. 22. The total summation of each line was calculated as 22.65 W, and the result of the total summation was 20.36 W with a loss of 2.29 W in comparison with each line summation. The loss of the summation can be attributed to the load variation. The lower lines from 11 to 16 exhibited reduced output power owing to the ground reflection. Regardless of the DC output power of each rectenna, the total output power was adequately conserved in the summation.

Table 6 summarizes the comparison of the obtained results with those of previous studies. We observed that although various DC output connections were studied to enhance the RF-DC conversion efficiency in total summation, the number of rectennas was limited owing to the non-linearity of each rectenna. Therefore, the combination of the DC-DC converter and Schottky diode facilitates the utilization of larger rectenna arrays.

IV. CONCLUSION

In this study, we employed a Schottky diode to enhance the DC power combination in an array rectenna. A DC-DC converter was adopted at the DC output port of the rectenna. The rectifier circuit exhibited an RF-DC conversion efficiency of 71% at an RF input level of 19 dBm and that of the 4 × 1 rectenna was 71.2% at 19.6 dBm. The single RHCP 4 × 8 rectenna exhibited an RF-DC conversion efficiency of 52.6% and 59.9% with and without the DC-DC converter, respectively. At an RF input level of 20.2 dBm, the DC output level measured using a four-stage doubler was 28 V. The Schottky diode was connected in series to the DC-DC converter at the backstage, thereby improving the level of DC power combining in the parallel-connected array rectenna system. The Schottky diode allows all DC-DC converters to operate under normal conditions and reduces the power loss in the DC power combining. The proposed rectenna structure can be extended to a larger array rectenna system with various input RF beamforming widths and shapes.

REFERENCES

[1] M. Yuan, R. Das, R. Ghannam, Y. Wang, J. Reboud, R. Fromme, F. Moradi, and H. Heidari, "Electronic contact lens: A platform for wireless health monitoring applications," *Adv. Intell. Syst.*, vol. 2, no. 4, Feb. 2020, Art. no. 1900190.
[2] P. Machura, V. D. Santis, and Q. Li, "Driving range of electric vehicles charged by wireless power transfer," *IEEE Trans. Veh. Technol.*, vol. 69, no. 6, pp. 5968–5982, Jun. 2020.
[3] H. Dinis, I. Colmiais, and P. M. Mendes, "Extending the limits of wireless power transfer to miniaturized implantable electronic devices," *Micromachines*, vol. 8, no. 12, p. 359, Dec. 2017.
[4] S. Bakogianni and S. Koulouridis, "A dual-band implantable rectenna for wireless data and power support at sub-GHz region," *IEEE Trans. Antennas Propag.*, vol. 67, no. 11, pp. 6800–6810, Nov. 2019.
[5] J. Alberto, C. Leal, C. Fernandes, P. A. Lopes, H. Paisana, A. T. D. Almeida, and M. Tavakoli, "Fully untethered battery-free biomonitoring electronic tattoo with wireless energy harvesting," *Sci. Rep.*, vol. 10, Mar. 2020, Art. no. 5539.
[6] B. Alzahrani and W. Ejaz, "Resource management for cognitive IoT systems with RF energy harvesting in smart cities," *IEEE Access*, vol. 6, pp. 62717–62727, Oct. 2018.
[7] W. Lee, Y. Jung, H. Jung, C. Seo, H. Choo, and H. Lee, "Wireless-powered chemical sensor by 2.4 GHz Wi-Fi energy-harvesting metamaterial," *Micromachines*, vol. 10, no. 1, p. 12, Dec. 2017.
[8] D. Li, Y. Zhou, Y. Cui, S. Huang, and D. Deng, "A wireless power transmission system with load regulation for implantable devices," *IEEE Trans. Instrum. Meas.*, vol. 23, no. 4, pp. 68–76, Jun. 2020.
[9] W. Lee and Y.-K. Yoon, "Wireless power transfer systems using metamaterials: A review," *IEEE Access*, vol. 8, pp. 147930–147947, Aug. 2020.
[10] I. Cash, "CASSIOPeiA—A new paradigm for space solar power," *Acta Astronaut.*, vol. 159, pp. 170–178, Jun. 2019.
[11] M. Wagih, G. S. Hilton, A. S. Weddell, and S. Beeby, "Broadband millimeter-wave textile-based flexible rectenna for wearable energy harvesting," *IEEE Trans. Microw. Theory Techn.*, vol. 68, no. 11, pp. 4960–4972, Nov. 2020.

[12] S. E. Rahaman and S. Dwari, "Circuit efficiency of high power amplifier circuit," *AEU, Int. J. Electron. Commun.*, vol. 123, Aug. 2020, Art. no. 153283.
[13] A. Mouapi, N. Hakem, and N. Kandil, "Performances comparison of Shottky voltage doubler rectifier to support RF energy harvesting," in *Proc. IEEE Int. Conf. Environ. Electr. Eng., IEEE Ind. Commercial Power Syst. Eur. (EEEIC/I&CPS Europe)*, Jun. 2020, pp. 1–5.
[14] S. Nektarios Daskalakis, A. Georgiadis, G. Goussetis, and M. M. Tentzeris, "A rectifier circuit insensitive to the angle of incidence of incoming waves based on a Wilkinson power combiner," *IEEE Trans. Microw. Theory Techn.*, vol. 67, no. 7, pp. 3210–3218, Jul. 2019.
[15] P. Saffari, A. Basaligheh, and K. Moez, "An RF-to-DC rectifier with high efficiency over wide input power range for RF energy harvesting applications," *IEEE Trans. Circuits Syst. I, Reg. Papers*, vol. 66, no. 12, pp. 4862–4875, Dec. 2019.
[16] A. Mouapi, "Performance analysis of multistage voltage doubler rectifier for RF energy harvesting," in *Proc. IEEE Int. Conf. Environ. Electr. Eng., IEEE Ind. Commercial Power Syst. Europe (EEEIC/I&CPS Europe)*, Jun. 2019, pp. 1–4.
[17] Y. Hu, S. Sun, H. Xu, and H. Sun, "Grid-array rectenna with wide angle coverage for effectively harvesting RF energy of low power density," *IEEE Trans. Microw. Theory Techn.*, vol. 67, no. 1, pp. 402–413, Jan. 2019.
[18] A. Bakytbekov, T. Q. Nguyen, C. Huynh, K. N. Salama, and A. Shamim, "Fully printed 3D cube-shaped multiband fractal rectenna for ambient RF energy harvesting," *Nano Energy*, vol. 53, pp. 587–595, Nov. 2018.
[19] X. Zhang, H. Liu, and L. Li, "Electromagnetic power harvester using wide-angle and polarization-insensitive metasurfaces," *Appl. Sci.*, vol. 8, no. 4, p. 497, Mar. 2018.
[20] W. Lin and R. W. Ziolkowski, "Electrically small, single-substrate Huygens dipole rectenna for ultracompact wireless power transfer applications," *IEEE Trans. Antennas Propag.*, vol. 69, no. 2, pp. 1130–1134, Feb. 2021.
[21] F. Khalid, W. Saeed, N. Shoaib, M. U. Khan, and H. M. Cheema, "Quad-band 3D rectenna array for ambient RF energy harvesting," *Int. J. Antennas Propag.*, vol. 2020, pp. 1–23, May 2020.
[22] Q. Chen, X. Chen, H. Cai, and F. Chen, "Schottky diode large-signal equivalent-circuit parameters extraction for high-efficiency microwave rectifying circuit design," *IEEE Trans. Circuits Syst. II, Exp. Briefs*, vol. 67, no. 11, pp. 2722–2726, Nov. 2020.
[23] K. Dang, J. Zhang, H. Zhou, S. Yin, T. Zhang, J. Ning, Y. Zhang, Z. Bian, J. Chen, X. Duan, S. Zhao, and Y. Hao, "Lateral GaN Schottky barrier diode for wireless high-power transfer application with high RF/DC conversion efficiency: From circuit construction and device technologies to system demonstration," *IEEE Trans. Ind. Electron.*, vol. 67, no. 8, pp. 6597–6606, Aug. 2020.
[24] J. Bae, S.-H. Yi, W. Choi, H. Koo, K. C. Hwang, K.-Y. Lee, and Y. Yang, "5.8 GHz high-efficiency RF–DC converter based on common-ground multiple-stack structure," *Sensors*, vol. 19, no. 15, p. 3257, Jul. 2019.
[25] H. Sun, H. He, and J. Huang, "Polarization-insensitive rectenna arrays with different power combining strategies," *IEEE Antennas Wireless Propag. Lett.*, vol. 19, no. 3, pp. 492–496, Mar. 2020.
[26] Y. Liu, K. Huang, Y. Yang, and B. Zhang, "A low-profile lightweight circularly polarized rectenna array based on coplanar waveguide," *IEEE Antennas Wireless Propag. Lett.*, vol. 17, no. 9, pp. 1659–1663, Sep. 2018.
[27] S. Lekshmi and O. Sheeba, "A review on novel designs for microwave power transmission using rectenna array," *Int. J. Eng. Res. Technol.*, vol. 9, no. 6, pp. 1393–1396, Jun. 2020.
[28] E. L. Chuma, Y. Iano, M. S. Costa, L. T. Manera, and L. L. B. Roger, "A compact-integrated reconfigurable rectenna array for RF power harvesting with a practical physical structure," *Prog. Electromagn. Res. M*, vol. 70, pp. 89–98, Jul. 2018.
[29] S. Shen and B. Clerckx, "Beamforming optimization for MIMO wireless power transfer with nonlinear energy harvesting: RF combining versus DC combining," *IEEE Trans. Wireless Commun.*, vol. 20, no. 1, pp. 199–213, Jan. 2021.
[30] H. Oraizi and S. Hedayati, "Miniaturization of microstrip antennas by the novel application of the Giuseppe Peano fractal geometries," *IEEE Trans. Antennas Propag.*, vol. 60, no. 8, pp. 3559–3567, Aug. 2012.
[31] T. Matsunaga, E. Nishiyama, and I. Toyada, "5.8-GHz stacked differential rectenna suitable for large-scale rectenna arrays with DC connection," *IEEE Trans. Antennas Propag.*, vol. 63, no. 12, pp. 5944–5949, Dec. 2015.
[32] Y. Yang, J. Li, L. Li, Y. Liu, B. Zhang, H. Zhu, and K. Huang, "A 5.8 GHz circularly polarized rectenna with harmonic suppression and rectenna array for wireless power transfer," *IEEE Antennas Wireless Propag. Lett.*, vol. 17, no. 7, pp. 1276–1280, Jul. 2018.

JEONG-MIN WOO received the B.Sc. degree in electronics from Kyungpook National University, South Korea, in 2011, and the M.Sc. degree in information and communication engineering and the Ph.D. degree in electrical and electronic computer engineering from the Gwangju Institute of Science and Technology, South Korea, in 2013 and 2016, respectively. He is currently a Senior Researcher with the Korea Electrotechnology Research Institute. His current research interests include wireless power transfer, metamaterial, compound semiconductor device, high power electromagnetic pulse protection, analysis of HVDC electrical environmental effect, and static electric field sensor.

WONSEOB LIM was born in Guri, South Korea, in 1987. He received the B.S. degree from the Department of Electronic and Communication Engineering, Hanyang University, Ansan, South Korea, in 2012, and the Ph.D. degree from the Department of Electrical and Computer Engineering, Sungkyunkwan University, Suwon, South Korea, in 2019.

Since 2018, he has been with the Korea Electro-Technology Research Institute (KERI), Ansan, where he is currently a Senior Engineer. His current research interests include the design of RF power amplifiers and wireless power transfer via microwaves for space solar power satellite.

JONGSEOK BAE was born in Suwon, South Korea, in 1987. He received the B.S. degree in electronic engineering from Chungnam University, Daejeon, South Korea, in 2014, and the Ph.D. degree from the Department of Electrical and Computer Engineering, Sungkyunkwan University, Suwon, in 2020.

Since 2020, he has been with the Department of Electrical and Computer Engineering, Sungkyunkwan University, where he designed power amplifiers. Since 2021, he has been with Qualcomm Korea RFFE, Seoul, Korea, where he is currently a Senior Engineer. His research interests include the design of RF/mm-wave power amplifiers, RF and analog integrated circuits, and microwave power transfer.

CHAN MI SONG received the B.S. degree in electronics and electrical engineering from Dongguk University, Seoul, South Korea, in 2015, and the Ph.D. degree from the Department of Electrical and Computer Engineering, Sungkyunkwan University, Suwon, South Korea, in 2021.

Her research interests include optimization of array antenna and microwave power transfer.

KYOUNG-JOO LEE received the B.S., M.S., and Ph.D. degrees in radio communication engineering from Korea University, Seoul, Korea, in 2006, 2009, and 2016, respectively. From 2007 to 2016, he was a Teaching Assistant with the Radio Communication Technology Laboratory, Korea University for Electromagnetic and Microwave Engineering. Since 2017, he has been a Postdoctoral Research Fellow Institute for research and development of microwave power transfer system for Space Solar Power System with the Korea Electrotechnology Research. His research interests include RF and microwave components, reconfigurable array antenna systems, wave propagation, RF energy harvesting, and microwave power transfer systems.

SANG-HWA YI (Member, IEEE) received the B.S. degree in electronic engineering from Korea University, Seoul, South Korea, in 2001, and the M.S. and Ph.D. degrees in microwave engineering from the Pohang University of Science and Technology (POSTECH), Pohang, South Korea, in 2003 and 2016, respectively.

Since 2003, he has been with the Korea Electro-technology Research Institute (KERI), where he developed various electromagnetic partial-discharge sensors for diagnosis of power apparatuses, including gas-insulated switchgears, transformers, and rotating machines. He is currently a Principal Researcher of the Power Grid Research Division, KERI, South Korea. His recent research interest includes large-scale wireless power transfer via microwaves for space solar power satellite.

Dr. Yi is a member of the IEEE DEI-Society, MTT-Society, and AP-Society. He was awarded the Korean Ministry of Trade, Industry and Energy's Commendation in invention day of 2020.

YOUNGOO YANG (Senior Member, IEEE) was born in Hamyang, South Korea, in 1969. He received the Ph.D. degree in electrical and electronic engineering from the Pohang University of Science and Technology, Pohang, South Korea, in 2002.

From 2002 to 2005, he was with Skyworks Solutions, Inc., Newbury Park, CA, USA, where he designed power amplifiers for various cellular handsets. Since 2005, he has been with the School of Information and Communication Engineering, Sungkyunkwan University, Suwon, South Korea, where he is currently a Professor. His current research interests include RF/mm-wave power amplifiers and RF transmitters.